Gas-Phase Reactions of Carbon Dioxide with Atomic Transition-Metal and Main-Group Cations: Room-Temperature Kinetics and Periodicities in Reactivity†

Gregory K. Koyanagi and Diethard K. Bohme*

Department of Chemistry, Centre for Research in Mass Spectrometry and Centre for Research in Earth and Space Science, York University, Toronto, Ontario, Canada, M3J 1P3

Received: May 20, 2005; In Final Form: July 29, 2005

The chemistry of carbon dioxide has been surveyed systematically with 46 atomic cations at room temperature using an inductively-coupled plasma/selected-ion flow tube (ICP/SIFT) tandem mass spectrometer. The atomic cations were produced at ca. 5500 K in an ICP source and allowed to cool radiatively and to thermalize by collisions with Ar and He atoms prior to reaction downstream in a flow tube in helium buffer gas at 0.35 ± 0.01 Torr and 295 ± 2 K. Rate coefficients and products were measured for the reactions of first-row atomic ions from K^+ to Se^+, of second-row atomic ions from Rb^+ to Te^+ (excluding Tc^+), and of third-row atomic ions from Cs^+ to Bi^+. CO_2 was found to react in a bimolecular fashion by O atom transfer only with 9 early transition-metal cations: the group 3 cations Sc^+, Y^+, and La^+, the group 4 cations Ti^+, Zr^+, and Hf^+, the group 5 cations Nb^+ and Ta^+, and the group 6 cation W^+. Electron spin conservation was observed to control the kinetics of O atom transfer. Addition of CO_2 was observed for the remaining 37 cations. While the rate of addition was not measurable some insight was obtained into the standard free energy change, $\Delta G°$, for CO_2 ligation from equilibrium constant measurements. A periodic variation in $\Delta G°$ was observed for first row cations that is consistent with previous calculations of bond energies $D_0(M^+-CO_2)$. The observed trends in D_0 and $\Delta G°$ are expected from the variation in electrostatic attraction between M^+ and CO_2 which follows the trend in atomic-ion size and the trend in repulsion between the orbitals of the atomic cations and the occupied orbitals of CO_2. Higher-order CO_2 cluster ions with up to four CO_2 ligands also were observed for 24 of the atomic cations while MO_2^+ dioxide formation by sequential O atom transfer was seen only with Hf^+, Nb^+, Ta^+, and W^+.

1. Introduction

Despite the global importance of carbon dioxide, surprisingly few experimental or theoretical investigations have been reported for the interactions of CO_2 with atomic metal cations. This can be attributed in part to earlier difficulties in generating atomic-metal cations in the gas phase for mass-spectrometric study and to earlier shortcomings associated with computational approaches. Consequently, previous experimental studies have been restricted to individual or small groups of atomic-metal cations. Only one systematic survey has been reported for the interactions of CO_2 with atomic metal cations using ab initio theory, and this was restricted to first-row transition-metal cations.

In early (1971) drift-tube and flowing- afterglow mass-spectrometer experiments, CO_2 was observed to add to alkali-metal cations Li^+, Na^+, and K^+ produced by thermionic surface-ionization emitters.[1] Apparently, the first measurement of a reaction of a transition-metal cation with CO_2 in the gas phase was that with Zr^+ reported in 1985 by Dheandhanoo et al.[2] Zr^+ ions were produced in a magnetically confined Penning discharge containing neon and $ZrBr_4$ and which was coupled to a selected-ion drift apparatus to measure rate coefficients. The measurements were made over an energy range from thermal energies (0.04 eV) to 0.3 eV (mean kinetic energy). Two sequential O atom transfer reactions, reactions 1 and 2, were observed to occur.

$$Zr^+ + CO_2 \rightarrow ZrO^+ + CO \quad (1)$$

$$ZrO^+ + CO_2 \rightarrow ZrO_2^+ + CO \quad (2)$$

Reaction 1 was reported to react with $k = 4.0 \times 10^{-10}$ cm^3 molecule^{-1} s^{-1} at 0.04 eV decreasing to 1×10^{-10} cm^3 molecule^{-1} s^{-1} at 0.3 eV. Reaction 2 was measured to proceed with $k = 1 \times 10^{-12}$ cm^3 molecule^{-1} s^{-1} at thermal energies, also decreasing with increasing ion energy.

The first metal-cation study using ion cyclotron resonance (ICR) mass spectroscopy, in which the metal cations were produced by laser volatilization/ionization, appears to have been published in 1991 by Irikura and Beauchamp who reported the following reaction sequence for tungsten cations with rate coefficients $k_3 = 6 \times 10^{-11}$ cm^3 molecule^{-1} s^{-1} and $k_4 = 2 \times 10^{-11}$ cm^3 molecule^{-1} s^{-1}, both estimated to be accurate to ± 25%.[3]

$$W^+ + CO_2 \rightarrow WO^+ + CO \quad (3)$$

$$WO^+ + CO_2 \rightarrow WO_2^+ + CO \quad (4)$$

Using similar techniques, Wesendrup and Schwarz[4] were able to show that, of the third-row metal ions Ta^+, W^+, Os^+, Ir^+, and Pt^+, only Ta^+ and W^+ form oxide cations in reactions with CO_2. These authors reported that reactions 5 and 6 occur at the

* Corresponding author. E-mail: dkbohme@yorku.ca. Telephone: 416-736-2100, ext 66188. Fax: 416-736-5936.

† Part of the special issue "William Hase Festschrift".

10.1021/jp0526602 CCC: $33.50
Published on Web 09/02/2005

collision rate, although no measured rate coefficients were reported.

$$Ta^+ + CO_2 \rightarrow TaO^+ + CO \quad (5)$$

$$TaO^+ + CO_2 \rightarrow TaO_2^+ + CO \quad (6)$$

Guided-ion beam mass spectrometry has been used to investigate the activation of CO_2 by U^+,[5a] Al^+,[5b] V^+,[5c] Fe_n^+ ($n = 1-18$),[5d] Nb^+,[5e] Cr_n^+ ($n = 1-18$),[5f] Mo^+,[5g] Y^+,[5h] Cu^+,[5i] Zr^+,[5j] and Pt^+.[5k,l] High-energy thresholds were reported for the onsets of MO^+ and MCO^+ production in the endothermic reactions of Al^+, Fe^+, Cr^+, Mo^+, Cu^+, and Pt^+ with CO_2. The reactions of U^+, Nb^+, Y^+, and Zr^+ were reported to proceed in an exothermic fashion by O atom transfer at, or close to, every collision near 0 eV, CM. A sharp minimum was observed in the cross section vs ion energy profile for VO^+ production with a cross section of 8×10^{-18} cm^2 at near 0 eV, CM. Also investigated was the activation of CO_2 by the monoxide cations UO^+,[5a] NbO^+,[5e] MoO^+,[5g] YO^+,[5h] ZrO^+,[5f] and PtO^+.[5k,j] Of these, only the reactions of NbO^+ and MoO^+ exhibit exothermic reaction behavior.

The clustering of carbon dioxide to FeO^+ according to reaction 7 has been observed with a selected-ion flow tube (SIFT) tandem mass spectrometer, but no reaction was seen between Fe^+ and CO_2, $k < 10^{-15}$ cm^3 molecule^{-1} s^{-1} in He at 0.35 Torr and 294 K.

$$FeO^+(CO_2)_n + CO_2 \rightarrow FeO^+(CO_2)_{n+1} \quad (n = 0-2) \quad (7)$$

However experimental studies of $Fe^+(CO_2)$ have been reported in which this ion is produced by ligand exchange reactions.[7]

Infrared photodissociation spectroscopy of CO_2 clusters of metal ions became possible with the development of supersonic molecular-beam machines combined with laser vaporization/ionization.[8] Cluster structures and intracluster reactions have been studied using this technique for a variety of main-group and transition-metal cations, $M^+(CO_2)_n$, with M = Mg, Al, Si, V, Fe, and Ni and n as large as 12 and more.[9] Resonant photodissociation spectroscopy with visible light has been used to characterize the bonding and structures of $V^+(CO_2)$, $Co^+(CO_2)$, $Ni^+(CO_2)$, and $ZrO^+(CO_2)$ produced in a laser-induced supersonic plasma.[10] Further insight into the binding energies and structures for $M^+(CO_2)$ with the first-row transition-metal atoms, has been provided by high level ab initio theory.[11]

Here we report an extensive experimental survey of the chemistry of 46 metal cations with CO_2 using ICP/SIFT tandem mass spectrometry in which the atomic-metal cations are produced in an inductively coupled plasma (ICP) of argon at ca. 5500 K. Rate coefficients are measured for all the observed primary reactions and the sequential higher-order chemistry was monitored as well. The formation of higher-order CO_2 clusters was also assessed for the establishment of equilibrium and this provides new measurements of the extent and strength of the binding of the CO_2 ligand to atomic-metal cations. Finally, since we have used the same technique previously to survey the reaction kinetics of the same 46 metal cations with the isoelectronic N_2O molecule,[12] we can provide a comparison of the kinetics for reactions with CO_2 with those of N_2O. This comparison leads to useful insight into comparisons of isoelectronic chemistry and the application of spin-selection rule as a criterion for predicting chemical reactivity.

2. Experimental Method

The experimental results reported here were obtained using the selected-ion flow tube (SIFT) tandem mass spectrometer described in detail elsewhere.[19] Recently, it has been modified to accept ions generated in an inductively coupled plasma (ICP) torch (ELAN series, Perkin-Elmer SCIEX) through an atmosphere/vacuum interface. The ICP ion source and interface have also been described previously.[13] Solutions containing the metal salt of interest having concentration of ca. 5 μg L^{-1} were peristaltically pumped via a nebulizer into the plasma. The nebulizer flow was adjusted to maximize the ion signal detected downstream of the flow tube. The sample solutions were prepared using atomic spectroscopy standard solutions commercially available from SPEX, Teknolab, J. T. Baker Chemical Co., Fisher Scientific Company, Perkin-Elmer, and Alfa Products. Aliquots of standard solutions were diluted with highly purified water produced in the Millipore Milli-Qplus ultrapure water system. Single-isotope solutions were used for M^+ (m/z) = Ca^+ (44), Se^+ (80), Zr^+ (90), Mo^+ (98), Ru^+ (102), Pd^+ (108), Cd^+ (112), Os^+ (192), and Pt^+ (195). Readily soluble compounds of these metals were obtained from Oak Ridge National Laboratory (Isotope Business Office). The final concentrations were varied between 5 and 20 ppm to achieve suitable intensity of the resultant ion beam. Normally, a stabilizing agent was added to each solution to prevent precipitation. That was either HNO_3 or HCl for acid-stabilized salts or KOH for those base-stabilized.

Atomic ions emerge from the ICP at a nominal ion temperature of 5500 K with corresponding Boltzmann state distributions. These distributions have been derived from available optical spectra[14,15] and reported by us previously for the two electronic spin states with the highest population at 5500 K.[16] Energy levels as high as 3.7 eV (3×10^4 cm^{-1}) were included in the calculations. The calculations show that excited states of the main group elemental cations except Ba^+ are high in energy and contribute little (never more than 10%) to the total ion population at 5500 K. The ground ^{2}S state of Ba^+ contributes 44% and the excited ^{2}D state 55% at 5500 K. The state distributions are more variable for the transition-metal cations. Excited states contribute 20% or less toward the populations of Cr^+, Mn^+, Ni^+, Cu^+, Zn^+, Rh^+, Pd^+, Ag^+, Cd^+ Re^+, Au^+, and Hg^+ and 50% or more toward the populations of Ti^+, Y^+, Zr^+, Nb^+, La^+, and Ir^+ with Sc^+, V^+, Fe^+, Co^+, Mo^+, Ru^+, Hf^+, Ta^+, W^+, and Pt^+ having intermediate distributions.

After extraction from the ICP, the plasma ions may experience both radiative electronic-state relaxation and collisional relaxation. The latter may occur already with argon as the extracted plasma cools upon sampling and then with He atoms in the flow tube (ca. 4×10^5 collisions with He) prior to the reaction region. The actual extent of electronic relaxation (either radiative or collisional) is not known and is difficult to assess except indirectly from observed chemistry. Almost all of the electronic states of the transition-metal ions have positive parity; electric dipole transitions between states of the same parity are forbidden (Laporte rule).[17] This means that radiative transitions between different states in metal cations can be achieved only by either magnetic dipole or electric quadrupole radiation. The probabilities for these transitions are very low,[18] and the resulting radiative lifetimes are of the order of seconds or larger. The time interval in the ICP/SIFT experiments between the exit of the ICP source and the entrance in the reaction region is ca. 20 ms, and therefore, no major modification of state distributions can occur in this time interval by forbidden radiative decay. That having been said, there were no indications of excited-

state effects in our previous measurements of reactions of atomic cations derived from the same ICP source with N_2O, except with Pt^+.[16] The many collisions experienced by the atomic cations with the quite polarizable Ar atoms as they emerge from the ICP and the ca. 10^4 collisions with He atoms in the flow tube (the helium buffer gas pressure was 0.35 ± 0.01 Torr) appear to be sufficient to provide for the thermalization of the excited states and ensure that the atomic ions reach a translational temperature equal to the tube temperature of 295 ± 2 K prior to entering the reaction region.. However, the exact extent of electronic relaxation is uncertain. Clues to the presence of excited electronic states of the atomic ions in the reaction region can be found in the products observed and the shape of the semilogarithmic decay of the reacting atomic ion upon addition of neutral reactant. A change in slope will appear in the measured semilogarithmic atomic-ion decay when the ground state and excited state react at different rates even when they give the same product ions. An excited-state effect cannot be seen when the products and reaction rates are the same for both the ground and excited states but in this case the experimental results do define the ground-state kinetics. Our growing experience has shown that excited states can reveal themselves when the ground state of the atomic ion reacts only slowly by termolecular addition and excited states react rapidly in a bimolecular fashion. As it happens, *all indications in the observed kinetics with* CO_2 suggest that the possible presence of excited state does not interfere with the observed ground-state reaction profiles.

The CO_2 reagent gas has a very high purity of 99.995% (Air Products) and was added without helium dilution. Reaction rate coefficients were determined in the usual manner using pseudo first-order kinetics.[19] The rate coefficients for the primary and consecutive reactions reported herein have an absolute accuracy estimated to be ±30%.

3. Results and Discussion

The reactions of CO_2 were measured with 46 atomic ions, including 29 transition-metal and 17 main-group cations. Both the primary and higher-order chemistries were monitored. Results obtained for the reactions of Sc^+, Fe^+, Y^+, and W^+ are shown in Figure 1. Table 1 summarizes the measured rate coefficients, reaction efficiencies, the primary products and the higher-order product ions. The reaction efficiency is taken to be equal to the ratio k/k_c, where k is the experimentally measured rate coefficient and k_c is the capture or collision rate coefficient. k_c was computed using the algorithm of the modified variational transition-state/classical trajectory theory developed by Su and Chesnavich[20a] with $\alpha(CO_2) = 2.911 \times 10^{-24}$ cm^3.[20b]

3.1. Primary Reactions. Only O atom transfer, reaction 8a, and adduct formation, reaction 8b, were observed as primary reaction channels, one or the other, but never both.

$$M^+ + CO_2 \rightarrow MO^+ + CO \quad (8a)$$

$$\rightarrow M^+(CO_2) \quad (8b)$$

As expected from the much lower first ionization energy of the transition and main-group metal atoms, IE(M), all ≤10.44 eV (see Table 2) and so less than that for CO_2 (13.773 ± 0.002 eV),[21] electron transfer was not observed with any of the M^+ cations.

O atom abstraction was observed only with 9 of the 46 atomic cations that were investigated. These are all early transition-metal cations (group 3, Sc^+, Y^+, and La^+; group 4, Ti^+, Zr^+, and Hf^+; group 5, Nb^+ and Ta^+; group 6, W^+). The rate coefficients measured for O atom abstraction are in the range 4.2×10^{-11} (for W^+) to 5.9×10^{-10} cm^3 molecule^{-1} s^{-1} (for Y^+).

CO_2 addition according to reaction 8b was observed for the remaining 37 late transition-metal and main group atomic cations. These addition reactions are expected to be termolecular with He buffer-gas atoms acting as the stabilizing third body; rate coefficients were not measured as a function of He pressure. The measured effective bimolecular rate coefficients for CO_2 addition all are lower limits because of the presence of back reaction.

Our measured reaction rate coefficients for O atom transfer to Zr^+, Ta^+, and W^+ can be compared with previously reported measurements. There is reasonable agreement in all cases. Our value of $(2.5 \pm 0.8) \times 10^{-10}$ cm^3 molecule^{-1} s^{-1} for Zr^+ is close to the value of 4×10^{-10} cm^3 molecule^{-1} s^{-1} obtained previously with a selected-ion drift apparatus at 0.04 eV.[2] Our value of $(2.4 \pm 0.7) \times 10^{-10}$ cm^3 molecule^{-1} s^{-1} ($k/k_c = 0.36$) for Ta^+ is somewhat lower than the previous report of this reaction proceeding at the collision rate in an ICR-MS.[4] Our value of $(4.2 \pm 1.3) \times 10^{-11}$ cm^3 molecule^{-1} s^{-1} for W^+ is in agreement, within the combined experimental uncertainties, with the value of $(6 \pm 25\%) \times 10^{-11}$ cm^3 molecule^{-1} s^{-1} also obtained with an ICR-MS.[3]

3.2. Periodicities in Reaction Efficiencies. Only the early transition-metal cations in each of the three rows exhibit O atom abstraction chemistry, two in the first, three in the second and four in the third row. The efficiency for O atom transfer peaks with the earliest transition-metal cation in each row: Sc^+ (d^1s^1), Y^+ (s^2), and La^+ (d^2) with $k/k_c = 0.087$, 0.80. and 0.61, respectively. The remaining 37 cations all add CO_2 with efficiencies less than 0.001 so that no apparent periodicity was apparent in the efficiency of CO_2 addition. An overview of the variation in reaction efficiency along the first, second, and third rows of the periodic table is provided in Figure 2.

3.3. Thermodynamics of O Atom Abstraction. The known O atom affinities of atomic cations that are summarized in Table 2 indicate that all of the nine observed O atom transfer reactions are exothermic: the nine atomic cations involved all have O atom affinities >159 kcal mol^{-1} which is much larger than $OA(CO) = 127.2 \pm 0.1$ kcal mol^{-1}.[21] The remaining 37 atomic cations all were observed to react slowly by CO_2 addition and, with the exceptions of V^+ and As^+, all have O atom affinities less than 127.2 kcal mol^{-1}, and this makes O atom transfer endothermic. Figure 3 shows how the reaction efficiency for O atom transfer from CO_2 varies with the O atom affinity for the 46 atomic cations investigated. There was no indication of VO^+ formation from V^+ or AsO^+ formation with As^+. The absence of exothermic O atom transfer from CO_2 to ground-state V^+ (X^5D) can be understood since this transfer reaction to form ground-state VO^+ ($X^3\Sigma$) is spin forbidden, as has been noted previously by Sievers et al.[5a] A similar situation applies to the reaction with As^+ (X^3P) to form AsO^+ ($X^1\Sigma$)[22] for which our experiments also indicate exclusive formation of the CO_2 adduct. Apparently no spin-allowed surfaces are accessible to either As^+ (X^3P) or V^+ (X^5D) that lead to exothermic O atom transfer.

Our failure to observe O atom transfer to V^+ (X^5D) is somewhat at odds with the sharp minimum observed in guided-ion beam experiments in the cross section vs ion energy profile for VO^+ production with a cross section of 8×10^{-18} cm^2 at near 0 eV, CM.[5c] However, the reported interpretation of this

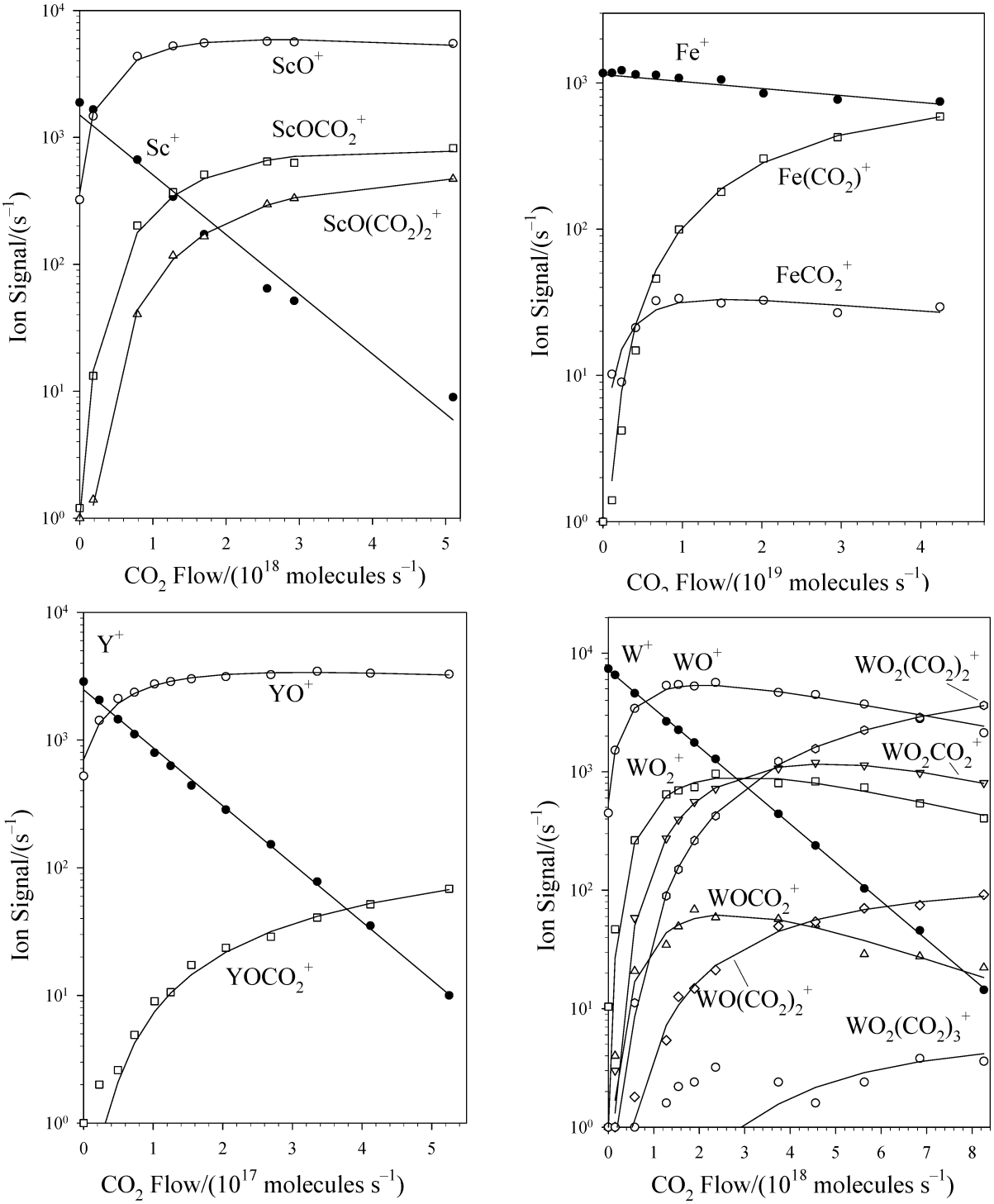

Figure 1. Composite of ICP/SIFT results for the reactions of the early first-row transition-metal ions Sc^+, Ti^+, Co^+, and As^+ with N_2O in helium buffer gas at 0.35±0.01 Torr and 295±2 K.

latter value was somewhat qualified: "the cross section shown is due exclusively to reaction of $V^+(a^5D)$ with CO_2 (presumably the authors mean X^5D), although O_2 and V^+ excited-state contamination cannot be ruled out with 100% confidence".[5c]

3.4. Comparison with O Atom Abstraction from N_2O. A comparison of O atom affinities shows that OA(CO) is 87 kcal mol^{-1} larger than $OA(N_2)$ so that endothermicity is much more constraining to O atom transfer from CO_2 than from N_2O. Indeed, many more O atom transfer reactions are exothermic between N_2O and the 46 metal cations that were investigated. The nine O atom transfer reactions observed with CO_2 also were all observed with N_2O,[12] but interesting differences are present in the measured rate coefficients and reaction efficiencies.

The two O atom transfer reactions with the first-row metal cations observed with both N_2O and CO_2 are much more efficient with N_2O than with CO_2: 0.73 vs 0.087 and 0.47 vs 0.049 for Sc^+ and Ti^+, respectively (Ti^+ also reacts with N_2O by N atom transfer but this has been factored out in this comparison).[12] Ground-state O atom transfer to both of these metal cations is spin forbidden from both N_2O and CO_2, but transfers from N_2O are more exothermic by 87 kcal mol^{-1}. So we may attribute the relatively low efficiencies observed for

TABLE 1: Rate Coefficients (in units of cm^3 molecule^{-1} s^{-1}), Reaction Efficiencies (k/k_c), and Higher-order Product Ions Measured for Reactions of Atomic Cations with Carbon Dioxide in Helium at 0.35 ± 0.01 Torr and 295 ± 2 K

reaction	k^a	$k_c{}^b$	k/k_c	higher-order product ions
$K^+ + CO_2 \rightarrow K^+ \cdot CO_2$	$\geq 9 \times 10^{-13}$	$8.8 \times 10-^{10}$	$\geq 1 \times 10^{-3}$	
$Ca^+ + CO_2 \rightarrow Ca^+ \cdot CO_2$	$\geq 5 \times 10^{-13}$	8.5×10^{-10}	$\geq 6 \times 10^{-4}$	
$Sc^+ + CO_2 \rightarrow ScO^+ + CO$	7.4×10^{-11}	8.5×10^{-10}	0.087	$ScO^+(CO_2)_{1,2}$
$Ti^+ + CO_2 \rightarrow TiO^+ + CO$	4.1×10^{-11}	8.3×10^{-10}	0.049	$TiO^+ \cdot CO_2$
$V^+ + CO_2 \rightarrow V^+ \cdot CO_2$	$\geq 5 \times 10^{-13}$	8.2×10^{-10}	$\geq 6 \times 10^{-4}$	$V^+(CO_2)_{2-4}$
$Cr^+ + CO_2 \rightarrow Cr^+ \cdot CO_2$	$\geq 6 \times 10^{-13}$	8.2×10^{-10}	$\geq 7 \times 10^{-4}$	$Cr^+(CO_2)_{2,3}$
$Mn^+ + CO_2 \rightarrow Mn^+ \cdot CO_2$	$\geq 5 \times 10^{-13}$	8.1×10^{-10}	$\geq 6 \times 10^{-4}$	$Mn^+(CO_2)_2$
$Fe^+ + CO_2 \rightarrow Fe^+ \cdot CO_2$	$\geq 5 \times 10^{-13}$	8.1×10^{-10}	$\geq 6 \times 10^{-4}$	$Fe^+(CO_2)_2$
$Co^+ + CO_2 \rightarrow Co^+ \cdot CO_2$	$\geq 5 \times 10^{-13}$	8.0×10^{-10}	$\geq 6 \times 10^{-4}$	$Co^+(CO_2)_2$
$Ni^+ + CO_2 \rightarrow Ni^+ \cdot CO_2$	$\geq 5 \times 10^{-13}$	8.0×10^{-10}	$\geq 6 \times 10^{-4}$	$Ni^+(CO_2)_{2,3}$
$Cu^+ + CO_2 \rightarrow Cu^+ \cdot CO_2$	$\geq 4 \times 10^{-13}$	8.0×10^{-10}	$\geq 5 \times 10^{-4}$	$Cu^+(CO_2)_2$
$Zn^+ + CO_2 \rightarrow Zn^+ \cdot CO_2$	$\geq 7 \times 10^{-13}$	7.7×10^{-10}	$\geq 9 \times 10^{-4}$	$Zn^+(CO_2)_2$
$Ga^+ + CO_2 \rightarrow Ga^+ \cdot CO_2$	$\geq 5 \times 10^{-13}$	7.7×10^{-10}	$\geq 6 \times 10^{-4}$	
$Ge^+ + CO_2 \rightarrow Ge^+ \cdot CO_2$	$\geq 9 \times 10^{-13}$	7.6×10^{-10}	$\geq 1 \times 10^{-3}$	$Ge^+(CO_2)_2$
$As^+ + CO_2 \rightarrow As^+ \cdot CO_2$	$\geq 1 \times 10^{-12}$	7.6×10^{-10}	$\geq 1 \times 10^{-3}$	$As^+(CO_2)_2$
$Se^+ + CO_2 \rightarrow Se^+ \cdot CO_2$	$\geq 5 \times 10^{-13}$	7.5×10^{-10}	$\geq 7 \times 10^{-4}$	
$Rb^+ + CO_2 \rightarrow Rb^+ \cdot CO_2$	$\geq 5 \times 10^{-13}$	7.4×10^{-10}	$\geq 7 \times 10^{-4}$	
$Sr^+ + CO_2 \rightarrow Sr^+ \cdot CO_2$	$\geq 6 \times 10^{-13}$	7.4×10^{-10}	$\geq 8 \times 10^{-4}$	$Sr^+(CO_2)_2$
$Y^+ + CO_2 \rightarrow YO^+ + CO$	5.9×10^{-10}	7.4×10^{-10}	0.80	$YO^+ \cdot CO_2$
$Zr^+ + CO_2 \rightarrow ZrO^+ + CO$	2.5×10^{-10}	7.4×10^{-10}	0.34	$ZrO^+(CO_2)_{1,2}$
$Nb^+ + CO_2 \rightarrow NbO^+ + CO$	1.8×10^{-10}	7.3×10^{-10}	0.25	NbO^+CO_2, $NbO_2{}^+(CO_2)_{0-3}$
$Mo^+ + CO_2 \rightarrow Mo^+ \cdot CO2$	$\geq 4 \times 10^{-13}$	7.3×10^{-10}	$\geq 5 \times 10^{-4}$	$Mo^+(CO_2)_2$,
$Ru^+ + CO_2 \rightarrow Ru^+ \cdot CO_2$	$\geq 4 \times 10^{-13}$	7.2×10^{-10}	$\geq 5 \times 10^{-4}$	$Ru^+(CO_2)_2$
$Rh^+ + CO_2 \rightarrow Rh^+ \cdot CO_2$	$\geq 4 \times 10^{-13}$	7.2×10^{-10}	$\geq 5 \times 10^{-4}$	$Rh^+(CO_2)_2$
$Pd^+ + CO_2 \rightarrow Pd^+ \cdot CO_2$	$\geq 4 \times 10^{-13}$	7.2×10^{-10}	$\geq 5 \times 10^{-4}$	$Pd^+(CO_2)_2$
$Ag^+ + CO_2 \rightarrow Ag^+ \cdot CO_2$	$\geq 5 \times 10^{-13}$	7.2×10^{-10}	$\geq 7 \times 10^{-4}$	$Ag^+(CO_2)_2$
$Cd^+ + CO_2 \rightarrow Cd^+ \cdot CO_2$	$\geq 6 \times 10^{-13}$	7.1×10^{-10}	$\geq 8 \times 10^{-4}$	
$In^+ + CO_2 \rightarrow In^+ \cdot CO_2$	$\geq 5 \times 10^{-13}$	7.1×10^{-10}	$\geq 7 \times 10^{-4}$	
$Sn^+ + CO_2 \rightarrow Sn^+ \cdot CO_2$	$\geq 6 \times 10^{-13}$	7.0×10^{-10}	$\geq 8 \times 10^{-4}$	
$Sb^+ + CO_2 \rightarrow Sb^+ \cdot CO_2$	$\geq 8 \times 10^{-13}$	7.0×10^{-10}	$\geq 1 \times 10^{-3}$	
$Te^+ + CO_2 \rightarrow Te^+ \cdot CO_2$	$\geq 6 \times 10^{-13}$	7.0×10^{-10}	$\geq 8 \times 10^{-4}$	
$Cs^+ + CO_2 \rightarrow Cs^+ \cdot CO_2$	$\geq 4 \times 10^{-13}$	7.0×10^{-10}	$\geq 6 \times 10^{-4}$	
$Ba^+ + CO_2 \rightarrow Ba^+ \cdot CO_2$	$\geq 6 \times 10^{-13}$	6.9×10^{-10}	$\geq 9 \times 10^{-4}$	$Ba^+(CO_2)_{2,3}$
$La^+ + CO_2 \rightarrow LaO^+ + CO$	4.2×10^{-10}	6.9×10^{-10}	0.61	$LaO^+ \cdot CO_2$
$Hf^+ + CO_2 \rightarrow HfO^+ + CO$	2.5×10^{-10}	6.7×10^{-10}	0.37	$HfO^+(CO_2)_{1,2}$
$Ta^+ + CO_2 \rightarrow TaO^+ + CO$	2.4×10^{-10}	6.7×10^{-10}	0.36	$TaO_2{}^+(CO_2)_{0-4}$
$W^+ + CO_2 \rightarrow WO^+ + CO$	4.2×10^{-11}	6.7×10^{-10}	0.063	$WO_2{}^+(CO_2)_{0-3}$
$Re^+ + CO_2 \rightarrow Re^+ \cdot CO_2$	$\geq 4 \times 10^{-13}$	6.7×10^{-10}	$\geq 6 \times 10^{-4}$	$Re^+(CO_2)_2$
$Os^+ + CO_2 \rightarrow Os^+ \cdot CO_2$	$\geq 6 \times 10^{-13}$	6.7×10^{-10}	$\geq 9 \times 10^{-4}$	$Os^+(CO_2)_{2,3}$
$Ir^+ + CO_2 \rightarrow Ir^+ \cdot CO_2$	$\geq 5 \times 10^{-13}$	6.7×10^{-10}	$\geq 7 \times 10^{-4}$	$Ir^+(CO_2)_{2,3}$
$Pt^+ + CO_2 \rightarrow Pt^+ \cdot CO_2$	$\geq 5 \times 10^{-13}$	6.7×10^{-10}	$\geq 7 \times 10^{-4}$	$Pt^+(CO_2)_2{}^+$
$Au^+ + CO_2 \rightarrow Au^+ \cdot CO_2$	$\geq 5 \times 10^{-13}$	6.7×10^{-10}	$\geq 7 \times 10^{-4}$	$Au^+(CO_2)_2{}^+$
$Hg^+ + CO_2 \rightarrow Hg^+ \cdot CO_2$	$\geq 5 \times 10^{-13}$	6.7×10^{-10}	$\geq 7 \times 10^{-4}$	
$Tl^+ + CO_2 \rightarrow Tl^+ \cdot CO_2$	$\geq 5 \times 10^{-13}$	6.6×10^{-10}	$\geq 7 \times 10^{-4}$	
$Pb^+ + CO_2 \rightarrow Pb^+ \cdot CO_2$	$\geq 5 \times 10^{-13}$	6.6×10^{-10}	$\geq 7 \times 10^{-4}$	$Pb^+(CO_2)_2{}^+$
$Bi^+ + CO_2 \rightarrow Bi^+ \cdot CO_2$	$\geq 4 \times 10^{-13}$	6.6×10^{-10}	$\geq 7 \times 10^{-4}$	$Bi^+(CO_2)_2{}^+$

[a] Effective bimolecular rate coefficient first-order in CO_2. The estimated uncertainty is ±30%. [b] Collision rate coefficient calculated using the algorithm of the modified variational transition-state/ classical trajectory theory developed by Su and Chesnavich.[20a]

the reactions with CO_2 to the greater availability of excited spin-allowed products in the reactions with N_2O.

For the second row, the relative values for O atom transfer from N_2O and CO_2 are as follows: 0.82 vs 0.80, 0.54 vs 0.34, and 0.54 vs 0.25 with Y^+, Zr^+, and Nb^+, respectively (with N atom transfer factored out). The efficiencies for the N_2O and CO_2 reactions are comparable, but the latter reactions, which are less exothermic by 87 kcal mol^{-1}, are up to two times less efficient. The latter two ground-state reactions with Zr^+ and Nb^+ are spin forbidden so that we can expect details of the potential-energy surfaces and crossings between them, for the most part unknown, to be rate determining.

The relative values for O atom transfer from N_2O and CO_2, respectively, with third-row atomic cations are as follows: 0.73 vs 0.61, 0.88 vs 0.37, 0.52 vs 0.36, and 0.85 vs 0.063 with La^+, Hf^+, Ta^+, and W^+, respectively (with N atom transfer factored out). The divergence in these efficiencies is substantial for the reactions with Hf^+ and more so for the reactions with W^+. Of these eight reactions only the two with Hf^+ are spin allowed. O atom transfer with the ground states of La^+, Ta^+, and W^+ is spin-forbidden to from ground-state products but may become spin-allowed for the formation of excited product MO^+ ions if sufficiently exothermic. This is not unlikely for the substantial exothermicities of these reactions, but is least likely with W^+ since this reaction is the least exothermic (by 39 ± 10 kcal mol^{-1}).

As we have noted already, all four of the ground-state O atom transfers from N_2O and CO_2 to V^+ and As^+ are exothermic and spin forbidden but seen only with N_2O at efficiencies of 0.27 and 0.83, respectively. This diverse behavior with these two isoelectronic molecules again can be understood since the two reactions of N_2O are more exothermic by 87 kcal mol^{-1} and so are likely to form spin-allowed excited metal−monoxide ion products.[12]

3.5. Dioxide Formation from MO^+. A second O atom abstraction, reaction 9, was observed with NbO^+, TaO^+, and

TABLE 2: O Atom Affinities, $D_0(M^+-O)$ in kcal mol^{-1}, and Ionization Energies, IE(M) in eV, for the Metal Ions Taken, with Few Exceptions, from the Review by Schröder et al.[23]

first row			second row			third row		
M^+	$OA(M^+)$	IE(M)	M^+	$OA(M^+)$	IE(M)	M^+	$OA(M^+)$	IE(M)
K^+	3	4.34	Rb^+	7	4.18	Cs^+	14	3.89
Ca^+	77.2	6.11	Sr^+	71.4	5.70	Ba^+	92.8	5.21
Sc^+	164.6 ± 1.4^a	6.56	Y^+	167.0 ± 4.2^b	6.22	La^+	206 ± 4^d	5.58
Ti^+	158.6 ± 1.6^a	6.83	Zr^+	178.9 ± 2.5^b	6.63	Hf^+	173 ± 5^e	6.83
V^+	134.9 ± 3.5^a	6.75	Nb^+	164.4 ± 2.5^b	6.76	Ta^+	188 ± 15^e	7.55
Cr^+	85.8 ± 2.8^a	6.77	Mo^+	116.7 ± 0.5^b	7.09	W^+	166 ± 10^f	7.86
Mn^+	68.0 ± 3.0^a	7.43				Re^+	115 ± 15^g	7.83
Fe^+	80.0 ± 1.4^a	7.90	Ru^+	87.9 ± 1.2^c	7.36	Os^+	100 ± 12^h	8.44
Co^+	74.9 ± 1.2^a	7.88	Rh^+	69.6 ± 1.4^c	7.46	Ir^+	59^e	8.97
Ni^+	63.2 ± 1.2^a	7.64	Pd^+	33.7 ± 2.5^c	8.34	Pt^+	$77,^i\ 75 \pm 2^j$	8.96
Cu^+	37.4 ± 3.5^a	7.72	Ag^+	28.4 ± 1.2^c	7.58	Au^+		9.23
Zn^+	38.5 ± 1.2^a	9.39	Cd^+		8.99	Hg^+		10.44
Ga^+	5.6	6.00	In^+		5.79	Tl^+		6.11
Ge^+	81.8	7.90	Sn^+	75.1	7.34	Pb^+	53.2	7.42
As^+	147 ± 2^k	9.81	Sb^+		8.64	Bi^+	41.6	7.29
Se^+	92^k	9.75	Te^+	96.6	9.01			

[a] Reference 24. [b] Reference 25. [c] Reference 26. [d] Reference 27. [e] Reference 21. [f] Reference 28. [g] Reference 29. [h] Reference 30. [i] Reference 31. [j] Reference 32. [k] Reference 22.

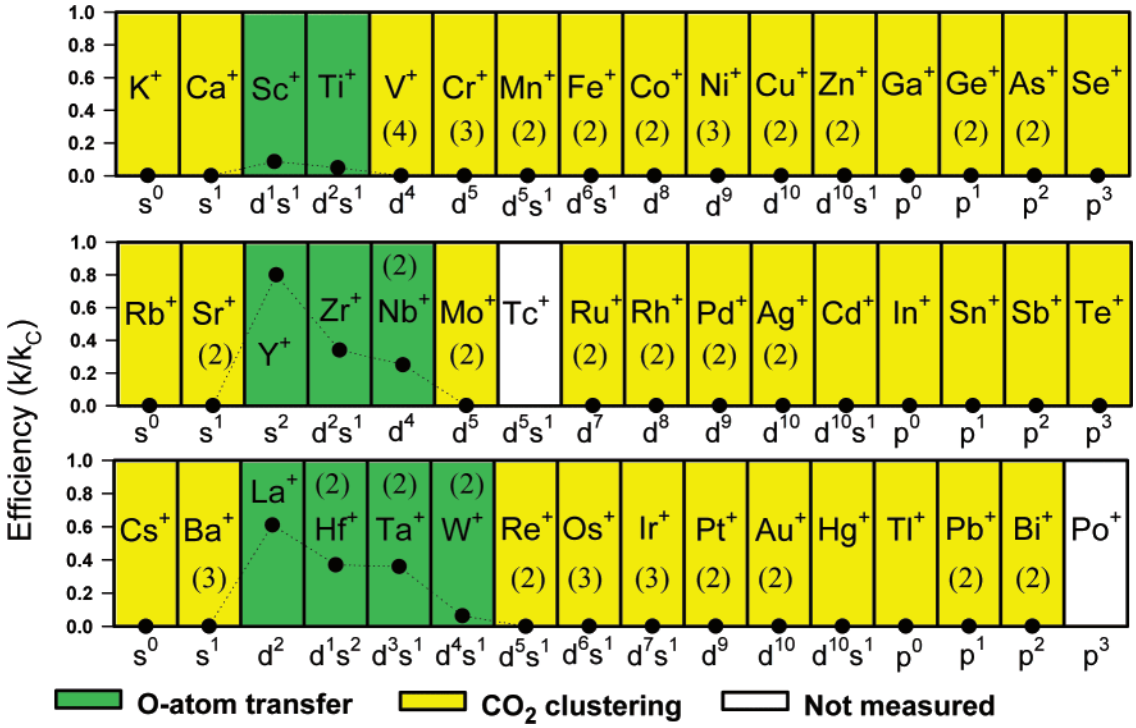

Figure 2. Periodic variations observed in the efficiencies, k/k_c (represented as solid circles), for reactions of atomic cations with carbon dioxide. k represents the measured reaction rate coefficient and k_c is the calculated collision rate coefficient (see Table 1). Also indicated are the observed reaction channels and the ground-state electronic configurations of the atomic cations. The reactions of Tc^+ and Po^+ were not investigated. The numbers in parentheses indicate the number of observed sequential reactions, either O atom transfer (green) or CO_2 clustering (yellow).

WO^+ with $k = 0.14 \times 10^{-10}$, 2.5×10^{-10}, and 0.084×10^{-10} cm^3 molecule^{-1} s^{-1}

$$MO^+ + CO_2 \rightarrow MO_2^+ + CO \qquad (9)$$

respectively. HfO^+ also was observed to form dioxide cations but only very slowly with $k = 5 \times 10^{-12}$ cm^3 molecule^{-1} s^{-1}. Reaction 9 is known to be exothermic with NbO^+, TaO^+, and WO^+ for which $D(O-MO^+) = 132$, 140, and 132 kcal mol^{-1}, respectively.[33] The most exothermic of these reactions is also the fastest. The O atom affinity of HfO^+ is not known. Sequential O atom transfer with CO_2 was observed to stop with the formation of the dioxide cation; higher oxide cations were not observed presumably because their formation is endothermic.

Comparisons can be made with previous kinetic results reported by others for reaction 9 with M = Y, Zr, Nb, Mo,Ta, and W and there is reasonable agreement. Our value of $(2.5 \pm 0.8) \times 10^{-10}$ cm^3 molecule^{-1} s^{-1} ($k/k_c = 0.35$) for Ta^+ is consistent with the previous report of reaction 9 with M = Ta proceeding at the collision rate in an ICR-MS.[4] Our value of $(8.4 \pm 2.5) \times 10^{-12}$ cm^3 molecule^{-1} s^{-1} for WO^+ is slightly lower than the value of $(2 \pm 25\%) \times 10-11$ cm^3 molecule^{-1} s^{-1} also obtained with an ICR-MS.[3] We did not observe the formation of ZrO_2^+ according to reaction 9, $k < 10^{-13}$ cm^3 molecule^{-1} s^{-1}, while the selected-ion drift measurements provided a value of 2.5 (+2.5, −1.25) $\times 10^{-12}$ cm^3 molecule^{-1}.[2] The origin of this discrepancy is not known; details

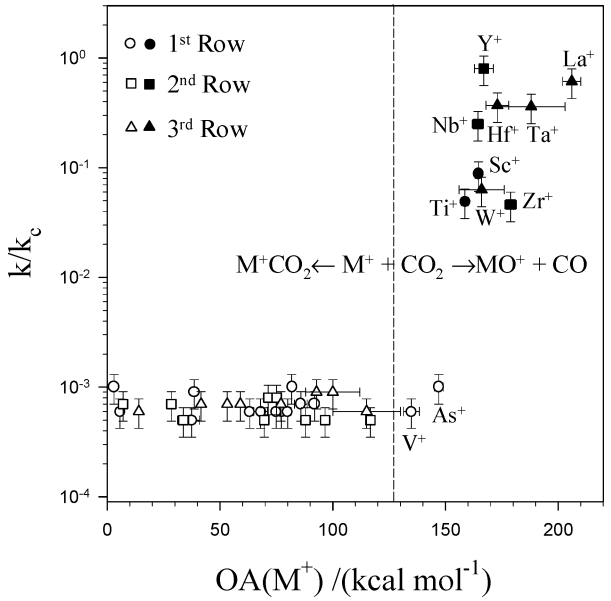

Figure 3. Dependence of the reaction efficiency, k/k_c, on the O atom affinity, OA, of the cation. k represents the measured reaction rate coefficient for loss of M^+ and k_c is the calculated collision rate coefficient (see Table 1). The dashed line represents OA(CO) = 127.2 ± 0.1 kcal mol^{-1}.[21] Reactions on the right of the dashed line are exothermic for O atom transfer while those on the left are endothermic. Solid points represent O atom transfer and open circles represent CO_2 addition. All open circles are *lower limits* to the reaction efficiency.

of the drift measurement were not reported, but our results are consistent with guided ion-beam measurements which indicate endothermic behavior for the reaction of ZrO^+ with CO_2.[5j] There is further agreement with previous guided ion-beam measurements for the reactions of NbO^+ and MoO^+ that were found to exhibit exothermic reaction behavior and the nonreaction of YO^+ that was found to be endothermic.[5e,g,h]

We have previously observed MO_2^+ dioxide formation with O_2[34] and N_2O.[12] The comparison with O_2 is interesting because of the similarities in exothermicities (OA(O) = 119.1 ± 0.1 kcal mol^{-1} vs OA(CO) = 127.2 ± 0.1 kcal mol^{-1}). O_2 was observed to transfer an O atom to NbO^+, MoO^+, TaO^+, and WO^+ compared to O atom transfer from CO_2 to HfO^+, NbO^+, TaO^+, and WO^+. There are two dissimilarities in these reactivities. HfO^+ adds O_2 to form HfO_3^+.[34] The failure of CO_2 compared to the ability of O_2 to transfer an O atom to MoO^+ suggests that 119.1 kcal mol^{-1} < OA(MoO^+) < 127.2 kcal mol^{-1}. Understandably more extensive and higher oxide formation was observed with N_2O because OA(N_2) is only 40 kcal mol^{-1}.

3.6. CO_2 Clustering. It seems that CO_2 addition to atomic ions has been seen previously in the gas phase only with some main-group and first-row transition-metal cations: Mg^+, Al^+, Si^+, V^+, Fe^+, Co^+, and Ni^+.[9,10] Some of these observations led to the spectroscopic measurement of M^+-CO_2 bond dissociation energies, and these are listed in Table 3. Also included in Table 3 are computed values for $D_0(M^+-CO_2)$ and a few additional experimental values obtained for $D_0(Fe^+-CO_2)$ by applying the bracketing technique to selected ligand-switching reactions.

The M^+-CO_2 bond dissociation energies summarized in Table 3 are quite low and range from ca. 10 to 25 kcal mol^{-1}. This translates to a range in standard free energies of ligation, reaction 8b, at room temperature from ca. −4 to −19 kcal mol^{-1} when the standard entropy change associated with the ligation is estimated at ca. −20 cal mol^{-1} deg^{-1} which is typical, within ±2 cal mol^{-1} deg^{-1}, for the electrostatic ligation of small

TABLE 3: Experimental and Computed Values for $D_0(M^+-CO_2)$ Binding Energies for First-Row Transition-Metal Cations

M^+	M^+-CO_2	method	ref
Sc^+	24.2	B3LYP	11
	20.7	CCSD(T) (ANO)	11
Ti^+	27.2	B3LYP	11
	21.1	CCSD(T) (ANO)	11
V^+	21.0	B3LYP	11
	18.2	CCSD(T) (ANO)	11
	17.3 ± 0.9	guided-ion beam MS	5(c)
Cr^+	19.5	B3LYP	11
	15.1	CCSD(T) (ANO)	11
Mn^+	13.5	B3LYP	11
	13.2	CCSD(T) (ANO)	11
Fe^+	17.0	B3LYP	11
	16.1	CCSD(T) (ANO)	11
	8 ± 2	FT-ICR MS	7(a)
	13.0 ± 1.3	FT-ICR MS	7(b)
	14.3 ± 0.9	guided-ion beam MS	7(c)
Co^+	24.5	B3LYP	11
	21.3	CCSD(T) (ANO)	11
	>20.0	photodissociation spectroscopy	10(b)
Ni^+	27.3	B3LYP	11
	24.2	CCSD(T) (ANO)	11
	24.9 ± 0.2	photodissociation spectroscopy	10(d)
Cu^+	24.3	B3LYP	11
	21.4	CCSD(T) (ANO)	11

molecules to atomic cations.[35] This corresponds to a range in equilibrium constants for the ligation reaction from ca. 10^3 to 10^{14} (standard state = 1 atm) at room temperature since $K = \exp(-\Delta G^\circ/RT)$. For the specific case of the CO_2 ligation of Fe^+ for which we can take a value for D_0 of 14 kcal mol^{-1},[7c] for example, we estimate a value for $\Delta G^\circ_{298} = -8$ kcal mol^{-1} which corresponds to an equilibrium constant at room temperature, $K = 6 \times 10^5$. Equilibrium constants with this approximate magnitude are measurable under the conditions of the flow tube experiments; values as large as 10^7 ($\Delta G^\circ_{298} = -10$ kcal mol^{-1}) can be measured in favorable cases.

The determination of an equilibrium constant for ligation reactions of type 8b is achieved at the fixed reaction time (9.4 ms) of our experiment with a plot of the ion signal ratio or ion concentration ratio, $[(M^+CO_2)]/[(M^+)]$, against the flow of CO_2 when this plot becomes linear and mass discrimination is taken into account. Only lower limits are accessible when equilibrium is not achieved in the reaction region either because of insufficient time or because a fast sequential addition to form a higher CO_2 cluster which prevents sufficient back reaction. Breakup of the adduct ion in the sampling process also will lead to lower limits for the true equilibrium constant. However, this latter effect will be most pronounced for the weakest bonds and should not be an issue for adduct ions with binding energies ≥5 kcal mol^{-1} at the short time the ions spend in the sampling region. Experiments with weak adduct ions and low rates of ligation required the addition of very large flows of CO_2. At these very high flows ($\geq 1 \times 10^{19}$ molecules s^{-1}) at which CO_2 becomes a significant proportion (≥0.3%) of the buffer gas, the signal of the atomic ions appeared to increase and negative curvature appeared in the equilibrium ratio plots. An illustrative ratio plot is shown in Figure 4. A number of effects come into play at such high flows of CO_2. Loss of ions to the wall by axial diffusion is reduced because of the presence of the heavier CO_2 molecules and perhaps more so for CO_2 cluster ions if they can transfer their atomic metal cation to the ambient CO_2 at long range. Also, the heavier CO_2 molecules may enhance collisional dissociation in the sampling region and the rate of

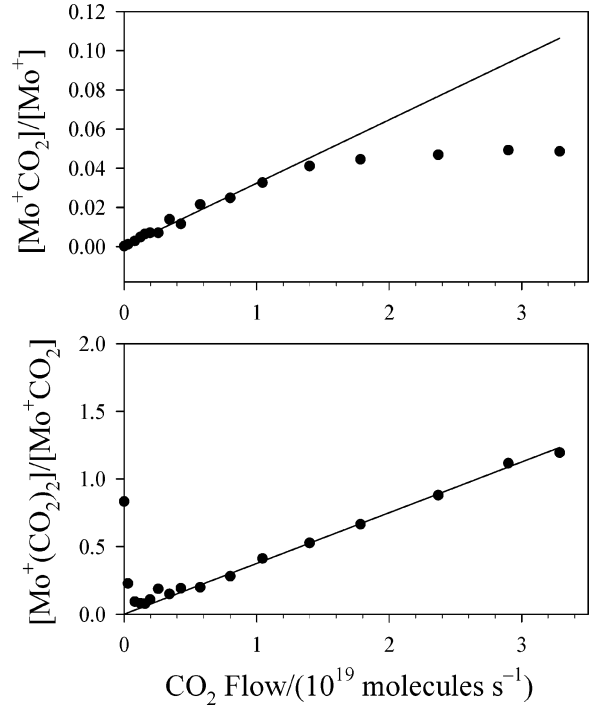

Figure 4. Ratio plots that illustrate the achievement of equilibrium. The curvature at high flows in the top figure is due to an observed rise in the Mo^+ signal which has been attributed to diffusion. The initial sharp curvature at low flows in the bottom figure is due to rapid occurrence of the second addition of CO_2.

the back reaction producing M^+ and so enhance the M^+ signal while reducing the cluster-ion signal and so introducing the negative curvature in the equilibrium ratio plot. As a consequence, equilibrium constants determined from linear plots that show negative curvature at high flows of CO_2 are treated as lower limits. The results of the equilibrium constant measurements are listed in Table 4.

Higher-order addition of CO_2 to atomic cations to form $M^+(CO_2)_2$ according to reaction 10 was observed in our experiments with the first-row cations $M^+ = V^+$, Cr^+, Mn^+, Fe^+, Co^+, Ni^+, Cu^+, and Zn^+, the second-row cations $M^+ = Sr^+$, Mo^+, Ru^+, Rh^+, Pd^+, and Ag^+, and the third-row cations $M^+ = Ba^+$, Re^+, Os^+, Ir^+, Pt^+, Au^+, Pb^+, and Bi^+. Formation of $M^+(CO_2)_3$ according to reaction 11 was observed only with $M^+ = V^+$, Cr^+, Ni^+, Ba^+, Os^+, and Ir^+.

$$M^+(CO_2) + CO_2 \rightarrow M^+(CO_2)_2 \quad (10)$$

$$M^+(CO_2)_2 + CO_2 \rightarrow M^+(CO_2)_3 \quad (11)$$

$V^+(CO_2)_4$ was the only fourth adduct that was observed. Table 1 includes a listing of all the higher-order CO_2 cluster ions that were observed and Table 4 includes equilibrium data for the formation of some diadducts and triadducts of CO_2. The higher-order chemistry initiated by Sc^+, Fe^+, Y^+, and W^+ can be tracked in Figure 1. Higher-order CO_2 clusters of atomic metal ions have been produced previously by laser vaporization in a pulsed nozzle cluster source. These include $Fe^+(CO_2)_n$ with $n = 1-14$,[9a] $V^+(CO_2)_n$ with $n = 1-11$,[9e] and $Ni^+(CO_2)_n$ with $n = 1-14$.[9f,g] It is interesting to note that four molecules of CO_2 were determined by infrared photodissociation spectroscopy to comprise the first solvation shell of both Ni^+ and V^+. This suggests that the four CO_2 molecules that were observed to add to V^+ under our experimental conditions have completed the first solvation shell in $V^+(CO_2)_4$.

TABLE 4: Standard Free Energy Changes ($\Delta G°$ in kcal mol^{-1}) and Measured Equilibrium Constants (K) for Sequential CO_2 Addition Reactions to M^+, MO^+, and MO_2^+ That Exhibit Equilibrium-like Kinetics under the Operating Conditions of the SIFT Experiments ($T = 295 \pm 2$ K) and Where Values Are Listed as $\Delta G°$ (K)[a]

M^+	0−1	1−2	2−3
K^+	−5.0 (4.4×10^3)		
Ca^+	−5.6 (1.4×10^4)		
V^+	−7.7 (4.1×10^5)	−8.5 (1.6×10^6)	−6.9 (1.1×10^5)
Cr^+	−6.4 (4.9×10^4)	−7.8 (5.1×10^5)	
Mn^+	−5.7 (1.4×10^4)		
Fe^+	≤−6.1 (≥3.0×10^4)	−9.0 (3.8×10^6)	
Co^+	≤−7.3 (≥2.3×10^5)	−9.3 (6.3×10^6)	
Ni^+	≤−6.8 (≥9.9×10^4)	−8.9 (3.2×10^6)	
Cu^+	≤−6.7 (≥8.1×10^4)	−8.6 (2.2×10^6)	
Zn^+	−6.0 (2.7×10^4)		
Ga^+	−4.9 (4.1×10^3)		
Ge^+	−6.2 (3.8×10^4)		
As^+	−7.9 (6.5×10^5)	−4.8 (3.1×10^3)	
Sr^+	−4.8 (3.2×10^3)		
Mo^+	≤−6.0 (≥2.6×10^4)	−7.5 (3.1×10^5)	
Ru^+	≤−6.0 (≥2.6×10^4)	−7.5 (3.4×10^5)	
Rh^+	≤−6.0 (≥2.6×10^4)	−7.5 (3.2×10^5)	
Pd^+	≤−5.9 (≥2.1×10^4)	−7.5 (2.9×10^5)	
Ag^+	≤−5.8 (≥1.9×10^4)	−6.7 (8.3×10^4)	
Cd^+	−5.1 (5.4×10^3)		
In^+	≤−3.9 (≥7.7×10^2)		
Sn^+	−4.9 (3.7×10^3)		
Sb^+	−5.3 (8.2×10^3)		
Cs^+	≤−1.6 (≥1.4×10^1)		
Ba^+	≤−5.2 (≥6.2×10^3)	≤−6.3 (≥4.2×10^4)	-4.5 (1.9×10^3)
Re^+	−4.8 (3.4×10^3)		
Pt^+	≤−6.4 (≥5.2×10^4)	≤−8.9 (≥3.1×10^6)	
Au^+	≤−6.2 (≥3.7×10^4)	≤−8.1 (≥9.4×10^5)	
Hg^+	−5.1 (5.4×10^3)		
Tl^+	−3.1 (1.9×10^2)		
Pb^+	≤−3.6 (≥4.3×10^2)		
Bi^+	≤−2.6 (≥8.1×10^1)		

MO^+	0−1	1−2
ScO^+	−7.5 (2.9×10^5)	−8.3 (1.2×10^6)
YO^+	−10.1 (2.5×10^7)	
ZrO^+	−7.7 (4.4×10^5)	
NbO^+	−6.4 (5.2×10^4)	
LaO^+	−6.1 (3.0×10^4)	
HfO^+	≤−7.4 (≥2.5×10^5)	−8.9 (3.7×10^6)
OsO^+	≤−9.2 (≥6.1×10^6)	≤−7.2 (≥2.0×10^5)

MO_2^+	0−1	1−2	2−3
NbO_2^+	≤−8.7 (≥2.2×10^6)	≤−9.8 (≥1.4×10^7)	
TaO_2^+	−8.9 (3.2×10^6)	−10.2 (3.2×10^7)	−8.6 (2.1×10^6)
WO_2^+	≤−8.6 (≥2.2×10^6)	≤−9.1 (≥4.5×10^6)	

[a] The estimated uncertainty in $\Delta G°$ is less than 0.3 kcal mol^{-1}. The estimated uncertainty in K is up to ±30%. Standard state = 1 atm.

Also included in Table 4 are equilibrium data obtained for the CO_2 clustering of some metal−oxide and metal−dioxide cations that was observed to occur according to reactions 12 and 13.

$$MO^+(CO_2)_n + CO_2 \rightarrow MO^+(CO_2)_{n+1} \quad (12)$$

$$MO_2^+(CO_2)_n + CO_2 \rightarrow MO_2^+(CO_2)_{n+1} \quad (13)$$

$ZrO^+(CO_2)$ has been synthesized previously in a molecular beam and spectroscopically characterized,[10e] as has $VO^+(CO_2)_n^+$ produced in a pulsed nozzle cluster source with $n = 1-10$.[9e] Furthermore, the clusters $FeO^+(CO_2)_{1,2}$ have been observed to be formed in reactions of type 5 with a selected-ion flow tube (SIFT) tandem mass spectrometer at 294 K.[6] The observation

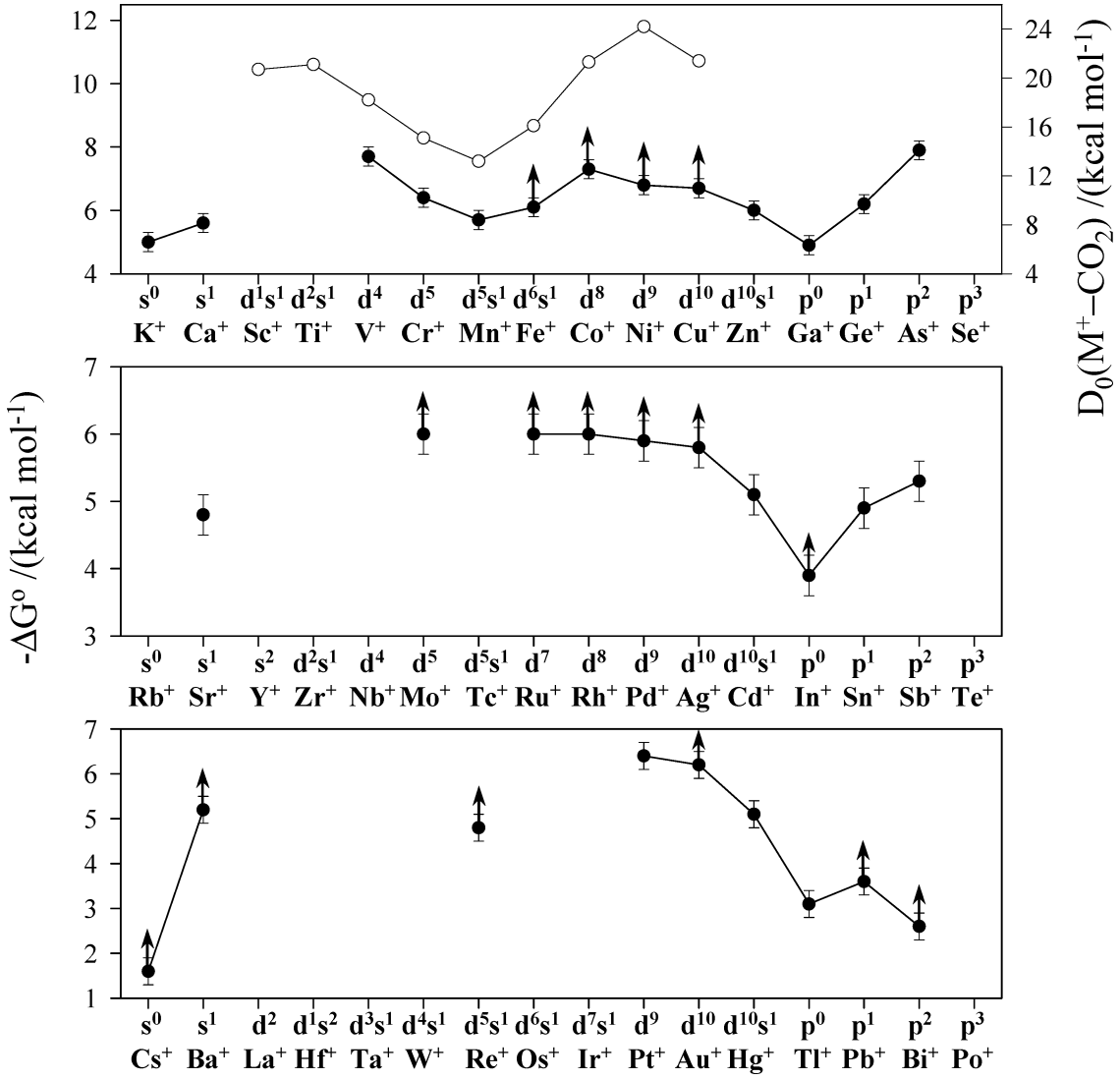

Figure 5. Variation in the standard free energy change, $\Delta G°$, for the addition of CO_2 to atomic-metal cations across the periodic table. Values for $\Delta G°$ are based on equilibrium constants measured under the operating conditions of the SIFT experiments ($T = 295 \pm 2$ K). Also indicated are bond dissociation energies (open circles, top right-hand scale) computed at the CCSD(T) (ANO) level of theory for first-row transition-metal cations.[11]

of $MO_2^+(CO_2)_n$ cluster ions also has been reported, but these were produced in mixtures of CO_2 and O_2.[9f] In the case of $ZrO^+(CO_2)$ and $NbO^+(CO_2)$ we can compare the reported values[5e,j] for $D_0(OZr^+-CO_2) = 0.74 \pm 0.06$ eV or 17 ± 1 kcal mol^{-1} and $D_0(ONb^+-CO_2) = 0.88 \pm 0.03$ eV or 20 ± 1 kcal mol^{-1} with our measured value for $\Delta G° = 7.7$ and 6.4 kcal mol^{-1}, respectively (see Table 4). When the standard entropy changes associated with the dissociations are estimated at ca. 20 cal mol^{-1} deg^{-1}, our values for $\Delta G°$ reduce to $\Delta H° = 14 \pm 2$ and 14 ± 2 kcal mol^{-1}, respectively, at 295 K.

3.7. Periodic Trends in the Standard Free Energy for CO_2 Ligation of M^+. Although the rate coefficients for the ligation of the atomic-metal cations with CO_2 were generally too small to measure with any accuracy, $k < \leq 9 \times 10^{-13}$ cm^3 molecule^{-1} s^{-1}, equilibrium constants, and therefore standard free energies of ligation, were more accessible to measurement. The latter are generally unknown from previous measurements with the exception of the computed and experimental values for $D_0(M^+\text{-}CO_2)$ listed in Table 3. Figure 5 explores the periodic variation in the values of $D_0(M^+-CO_2)$ and $\Delta G°$ listed in Tables 3 and 4, respectively, for the addition of CO_2 to M^+. Some clear trends are apparent and, for the first-row transition-metal cations, there is good correspondence between the periodic behavior of $\Delta G°$ and $D_0(M^+-CO_2)$. Both are not unexpected. The correspondence between the periodic behavior of $\Delta G°$ and $D_0(M^+-CO_2)$ is expected since $\Delta(\Delta S°) \approx 0$ for the family of similar CO_2 addition reactions with transition-metal cations since $\Delta(\Delta G°) \approx \Delta(\Delta H°) \approx \Delta(D_0(M^+-CO_2))$. The periodic trend in the calculated values for $D_0(M^+-CO_2)$ for first-row transition-metal ions is similar to the periodic trends in experimental values for $D_0(M^+\text{-L})$ reported previously for other ligands such as water, ammonia, benzene, imidazole, and adenine.[36]

As has been noted previously,[11] cationic metals are bound to CO_2 electrostatically in an end-on (η^1-O) coordination since CO_2 has a negative quadrupole moment. The electrostatic interaction between the atomic-metal cation and CO_2 has been computed to produce only small asymmetry in the two CO bond lengths which remains almost constant across the first row.[11] There is no significant π-back-donation from the metal cation to CO_2. The M^+-CO_2 bond distances are determined both by the size of the ion, which decreases across the row, and by the metal−ligand repulsion, which depends on the electronic configuration of the metal cation.[11] The M^+-CO_2 binding energies across the first row of the periodic table are similarly determined by

the trend in electrostatic attraction which follows the trend in ion size and the trend in repulsion between the metal d orbitals and the occupied orbitals of CO_2, the order of repulsion being $3d\sigma > 3d\pi > 3d\delta$. Minima in D_0 or $\Delta G°$ appear for $Mn^+(3d^54s^1)$ and $Ga^+(3d^{10}4s^24p^0)$ where the repulsion is largest. The increase in M^+-CO_2 attraction due to decreasing size determines the trend in increasing bond energy observed just beyond Mn^+ and Ga^+ and also beyond In^+.

4. Conclusions

A systematic survey of the room-temperature ground-state chemistry of 46 metal cations has shown that carbon dioxide reacts in a bimolecular fashion by O atom transfer only with 9 early transition-metal cations: the group 3 cations Sc^+, Y^+, and La^+, the group 4 cations Ti^+, Zr^+, and Hf^+, the group 5 cations Nb^+ and Ta^+, and the group 6 cation W^+. The efficiencies for O atom abstraction are in the range 0.046 (for Zr^+) to 0.80 (for Y^+). Thermodynamics and spin play a role in controlling the kinetics and product formation in O atom transfer reactions of atomic-metal cations with CO_2, just as we had found previously for O atom transfer from the isoelectronic N_2O molecule to the same metal cations.[11] MO_2^+ dioxide formation by sequential O atom transfer occurs only with Hf^+, Nb^+, Ta^+, and W^+.

Addition of CO_2 occurs under SIFT conditions with 37 cations, those that do not react by O atom transfer. The standard free energy change $\Delta G°$ for CO_2 ligation, as determined from equilibrium constant measurements, shows a periodic variation. For first row cations this variation is consistent with previous calculations of M^+-CO_2 bond energies and what is expected from the variation in electrostatic attraction between M^+ and CO_2. The latter follows the trend in atomic-ion size and the trend in repulsion between the orbitals of the atomic cations and the occupied orbitals of CO_2. Higher-order CO_2 cluster ions with up to four CO_2 ligands are formed under SIFT conditions with 24 of the atomic cations.

Acknowledgment. Continued financial support from the Natural Sciences and Engineering Research Council of Canada is greatly appreciated. Also, we acknowledge support from the National Research Council, the Natural Science and Engineering Research Council and MDS SCIEX in the form of a Research Partnership grant. As holder of a Canada Research Chair in Physical Chemistry, D.K.B. thanks the contributions of the Canada Research Chair Program to this research.

References and Notes

(1) (a) Keller, G. E.; Beyer, R. A. *J. Geophys. Res.* **1971**, *76*, 289. (b) Keller, G. E.; Beyer, R. A. *Trans. Am. Geophys. Union Res.* **1971a**, *52*, 303. (c) Perry, R. A.; Rowe, B. R.; Viggiano, A. A.; Albritton, D. L.; Ferguson, E. E.; Fehsenfeld, F. C. *Geophys. Res. Lett.* **1980**, *7*, 693.

(2) Dheandhanoo, S.; Chatterjee, B. K.; Johnson, R. *J. Chem. Phys.* **1985**, *83*, 3327.

(3) Irikura, K. K.; Beauchamp, J. L. *J. Phys. Chem.* **1991**, *95*, 8344.

(4) Wesendrup, R.; Schwarz, H. *Angew. Chem., Int. Ed. Engl.* **1995**, *34*, 2033.

(5) (a) Armentrout, P. B.; Beauchamp, J. L. *Chem. Phys.* **1980**, *50*, 27. (b) Clemmer, D. E.; Weber, M. E.; Armentrout, P. B. *J. Phys. Chem.* **1992**, *96*, 10888. (c) Sievers, M. R.; Armentrout, P. B. *J. Chem. Phys.* **1995**, *102*, 754. (d) Griffin, J. B.; Armentrout, P. B. *J. Chem. Phys.* **1997**, *107*, 5345 (e) Sievers, M. R.; Armentrout, P. B. *Int. J. Mass Spectrom.* **1998**, *179/180*, 103. (f) Griffin, J. B.; Armentrout, P. B. *J. Chem. Phys.* **1998**, *108*, 8075. (g) Sievers, M. R.; Armentrout, P. B. *J. Phys. Chem. A.* **1998**, *102*, 10754. (h) Sievers, M. R.; Armentrout, P. B. *Inorg. Chem.* **1999**, *38*, 397. (i) Rodgers, M. T.; Walker, B.; Armentrout, P. B. *Int. J. Mass Spectrom.* **1999**, *182/183*, 99. (j) Sievers, M. R.; Armentrout, P. B. *Int. J. Mass Spectrom.* **1999**, *185/186/187*, 117. (k) Zhang, X.-G.; Armentrout, P. B. *J. Phys. Chem. A* **2003**, *107*, 8904. (l) Zhang, X.-G.; Armentrout, P. B. *J. Phys. Chem. A* **2003**, *107*, 8915.

(6) Baranov, V.; Javahery, G.; Hopkinson, A. C.; Bohme, D. K. *J. Am. Chem. Soc.* **1995**, *117*, 12801.

(7) (a) Schwarz, J.; Schwarz, H. *Organometallics* **1994**, *13*, 1518. (b) Dieterle, M.; Harvey, J. N.; Heinemann, C.; Schwarz, J.; Schrder, D.; Schwarz, H. *Chem. Phys. Lett.* **1997**, *277*, 399. (c) Tjelta, B. L.; Walter, D.; Armentrout, P. B. *Int. J. Mass Spectrom.* **2001**, *204*, 7.

(8) (a) Weinheimer, C. J.; Lisy, J. M. *J. Phys. Chem.* **1996**, *100*, 15305. (b) Weinheimer, C. J.; Lisy, J. M. *Chem Phys.* **1998**, *239*, 357.

(9) (a) Gregoire, G.; Duncan, M. A. *J. Chem. Phys.* **2002**, *117*, 2120. (b) Gregoire, G.; Brinkmann, N. R.; van Heijnsbergen, Schaefer, H. F.; Duncan, M. A. *J. Phys. Chem. A* **2003**, *107*, 218. (c) Walters. R. S.; Brinkmann, N. R.; Schaefer, H. F.; Duncan, M. A. *J. Phys. Chem. A* **2003**, *107*, 7396. (d) Jaeger, J. B.; Jaeger, T. D.; Brinkmann, N. R.; Schaefer, H. F.; Duncan, M. A. *Can. J. Chem.* **2004**, *82*, 934. (e) Walker, N. R.; Walters. R. S.; Duncan, M. A. *J. Chem. Phys.* **2004**, *120*, 10037. (f) Walker, N. R.; Grieves, G. A.; Walters, R. S.; Duncan, M. A. *Chem. Phys. Lett.* **2003**, *380*, 230. (g) Walker, N. R.; Walters. R. S.; Grieves, G. A.; Duncan, M. A. *J. Chem. Phys.* **2004**, *121*, 10498.

(10) (a) Lessen, D. E.; Asher, R. L.; Brucat, P. J. *J. Chem. Phys.* **1991**, *95*, 1414. (b) Asher, R. L.; Bellert, D.; Buthelezi, T.; Brucat, P. J. *Chem. Phys. Lett.* **1994**, *227*, 623. (c) Bellert, D.; Buthelezi, T.; Brucat, P. J. *Chem. Phys.* Lett. **1998**, *290*, 316. (d) Asher, R. L.; Bellert, D.; Buthelezi, T.; Weerasekera, G.; Brucat, P. J. *Chem. Phys. Lett.* **1994**, *228*, 390. (e) Bellert, D.; Buthelezi, T.; Hayes, T.; Brucat, P. J. *Chem. Phys. Lett.* **1997**, *276*, 242.

(11) Sodupe, M.; Branchadell, V.; Rosi, M.; Bauschlicher, C. W. *J. Phys. Chem.* **1997**, *101*, 7854.

(12) Lavrov, V. V.; Blagojevic, V.; Koyanagi, G. K.; Orlova, G.; Bohme, D. K. *J. Phys. Chem. A* **2004**, *108*, 5610.

(13) (a) Koyanagi, G. K.; Lavrov, V.; Baranov, V. I.; Bandura, D.; Tanner, S. D.; McLaren, J. W.; Bohme, D. K. *Int. J. Mass Spectrom.* **2000**, *194*, L1. (b) Koyanagi, G. K.; Baranov, V. I.; Tanner, Bohme, D. K. *J. Anal. At. Spectrom.* **2000**, *15*, 1207.

(14) Moore, C. E. *Atomic energy levels as derived from the analyses of optical spectra*; U.S. National Bureau of Standards: Washington, DC, 1971.

(15) Van Kleef, Th. A. M.; Metsch, B. C. *Physica* **1978**, *C 95*, 251.

(16) Lavrov, V. V.; Blagojevic, V.; Koyanagi, G. K.; Bohme, D. K. *J. Phys. Chem. A* **2004**, *108*, 5610.

(17) Condon, E. U.; Shortley, G. H. *The theory of atomic spectra*; Cambridge University Press: Cambridge, U.K., 1963; pp 236−237.

(18) Garstang, R. H. *Mon. Not. R. Astron. Soc.* **1962**, *124*, 321.

(19) (a) Mackay, G. I.; Vlachos, G. D.; Bohme, D. K.; Schiff, H. I. *Int. J. Mass Spectrom. Ion Phys.* **1980**, *36*, 259. (b) Raksit, A. B.; Bohme, D. K. *Int. J. Mass Spectrom. Ion Processes* **1983/84**, *55*, 69.

(20) (a) Su, T.; Chesnavich, W. J. *J. Chem. Phys.* **1982**, *76*, 5183. (b) *Handbook of Chemistry and Physics*, 78th ed.; CRC Press: Boca Raton, FL, 1997.

(21) Lias, S. G.; Bartmess, J. E.; Liebman, J. F.; Holmes, J. L.; Levin, R. D.; Mallard, W. G. *J. Phys. Chem. Ref. Data* **1988**, *17*, Suppl 1.

(22) S. Petrie, private communications. The calculations were done using the QCISD(T)/6-311+G(3df) method; the value for $OA(Se^+)$ does not include a spin−orbit correction.

(23) Schröder, D.; Schwarz, H.; Shaik, S. *Structure and Bonding (Berlin)*; Springer-Verlag: Berlin, and Heidelberg, Germany, 2000; Vol 97, pp 91−122.

(24) Freiser, B. S., Ed. *Organometallic ion chemistry*; Kluwer: Dordrecht, The Netherlands, 1996.

(25) Sievers, M. R.; Chen, Y.-M.; Armentrout, P. B. *J. Chem. Phys.* **1996**, *105*, 6322.

(26) Chen, Y.-M.; Armentrout, P.B. *J. Chem. Phys.* **1995**, *103*, 618.

(27) Clemmer, D. E.; Dalleska, N. F.; Armentrout, P. B. *Chem. Phys. Lett.* **1992**, *190*, 259.

(28) Blagojevic, V.; Lavrov, V. V.; Orlova, G.; Bohme, D. K. *Chem. Phys. Lett.* **2004**, *389*, 303.

(29) Beyer, M. Dissertation, Technical University München, 1996.

(30) Irikura, K. K.; Beauchamp, J. L. *J. Am. Chem. Soc.* **1989**, *111*, 75.

(31) Pavlov, M.; Blomberg, M. R. A.; Siegbahn, P. E. M.; Wesendrup, R.; Heinemann, C.; Schwarz, H. *J. Phys. Chem. A* **1997**, *101*, 1567.

(32) Zhang, X.-G.; Armentrout, P. B. *J. Phys. Chem. A* **2003**, *107*, 8904.

(33) Schröder, D.; Schwarz, H.; Shaik, S. *Structure and Bonding (Berlin)*; Springer-Verlag: Berlin, and Heidelberg, Germany, 2000; Vol. 97, pp 91−122.

(34) Koyanagi, G. K.; Caraiman, D.; Blagojevic, V.; Bohme, D. K. *J. Phys. Chem. A* **2002**, *106*, 4581.

(35) Kebarle, P. *Annu. Rev. Phys. Chem.* **1977**, *28*, 445.

(36) Rodgers, M. T.; Armentrout, P. B. *Acc. Chem. Res.* **2004**, *37*, 989.